Target-Mounted Intelligent Reflecting Surface for Secure Wireless Sensing

Xiaodan Shao, Member, IEEE, and Rui Zhang, Fellow, IEEE

Abstract—In this paper, we consider a challenging secure wireless sensing scenario where a legitimate radar station (LRS) intends to detect a target at unknown location in the presence of an unauthorized radar station (URS). We aim to enhance the sensing performance of the LRS and in the meanwhile prevent the detection of the same target by the URS. Under this setup, conventional stealth-based approaches such as wrapping the target with electromagnetic wave absorbing materials are not applicable, since they will disable the target detection by not only the URS, but the LRS as well. To tackle this challenge, we propose in this paper a new target-mounted IRS approach, where intelligent reflecting surface (IRS) is mounted on the outer/echo surface of the target and by tuning the IRS reflection, the strength of its reflected radar signal in any angle of departure (AoD) can be adjusted based on the signal's angle of arrival (AoA), thereby enhancing/suppressing the signal power towards the LRS/URS, respectively. To this end, we propose a practical protocol for the target-mounted IRS to estimate the LRS/URS channel and waveform parameters based on its sensed signals and control the IRS reflection for/against the LRS/URS accordingly. Specifically, we formulate new optimization problems to design the reflecting phase shifts at IRS for maximizing the received signal power at the LRS while keeping that at the URS below a certain level, for both the cases of short-term and long-term IRS operations with different dynamic reflection capabilities. To solve these non-convex problems, we apply the penalty dual decomposition method to obtain high-quality suboptimal solutions for them efficiently. Finally, simulation results are presented that verify the effectiveness of the proposed protocol and algorithms for the target-mounted IRS to achieve secure wireless sensing, as compared with various benchmark schemes.

Index Terms—Target-mounted IRS, wireless sensing, sensing security, passive beamforming.

I. Introduction

The future sixth-generation (6G) wireless networks are envisioned as an enabler for various emerging applications, such as extended reality, tactile internet, intelligent transportation, massive Internet of Things (IoT), etc. [?]. These applications generally require extraordinarily high communication rate and/or reliability, as well as highly accurate sensing. Moreover, with the growing demand of wireless communication system capacity, spectrum/hardware resources are becoming increasingly scarce. The above trends have motivated a new research paradigm, called integrated sensing and communications (ISAC), for enabling sensing and communication functions in the same wireless network by sharing its platform and resources such as base station (BS), antenna, spectrum, waveform, etc. and jointly designing their operations to achieve balanced performance [?], [?], [?], [?]. It is thus anticipated that wireless sensing, which aims to accurately and efficiently detect, estimate, and extract useful physical information/features of environmental targets by exploiting radio wave transmission, reflection, diffraction, and scattering, will become a major service provided by 6G wireless networks, in addition to communications.

However, existing wireless sensing systems such as cellular BS sensing still face practical challenges. For example, the sensing range/accuracy of the radar (BS) is practically limited due to the high round-trip radar signal propagation loss between the radar and its sensing target as well as the target's finite radar cross section (RCS). Even under the line-of-sight (LoS) condition, when the radar-target distance is long and/or the RCS of the target is small, the echo signal received by the radar receiver is of low power, which degrades the sensing performance (e.g., target detection probability) against the background noise. Although this issue can be partially resolved by increasing the radar signal power and/or employing multiple-input-multiple-output (MIMO) radars, such conventional methods usually require substantially more energy consumption and higher implementation cost.

In recent years, intelligent reflecting surface (IRS) has been proposed as a promising new technology to achieve smart and reconfigurable signal propagation for wireless communications [?], [?]. Typically, IRS is a planar surface composed of a large number of low-cost passive reflecting elements, and by jointly adjusting the amplitude and/or phases of IRS elements, the direction and strength of the electromagnetic wave reflected by IRS can be flexibly controlled (i.e., passive beamforming). Motivated by the significant performance gains that IRS brings for wireless communications, recent studies have also revealed the great potential of IRS for enhancing the performance of wireless sensing [?], [?], [?], [?] as well as improving the communication-sensing trade-off for ISAC systems [?], [?], [?]. In these works, IRS is employed as additional anchor node in wireless network for improving the BS's detection accuracy, which, however, may not perform well in practice due to the significant path loss of the radar signal that is reflected by both the target (once) and

X. Shao is with the School of Science and Engineering, Chinese University of Hong Kong, Shenzhen, China 518172, (e-mail: shaoxiaodan@zju.edu.cn).

R. Zhang is with School of Science and Engineering, Shenzhen Research Institute of Big Data, The Chinese University of Hong Kong, Shenzhen, Guangdong 518172, China. He is also with the Department of Electrical and Computer Engineering, National University of Singapore, Singapore 117583 (e-mail: elezhang@nus.edu.sg).

the IRS (twice) before being received by the radar/BS receiver. To overcome this issue, in [?] and [?], the authors proposed a new IRS active sensing approach, where the IRS (instead of cellular BS) directly sends radar signal, and sensors installed on the IRS receive the echo reflected by the target for detection, thus avoiding the severe (double) path loss between the sensing/ISAC BS and IRS in conventional IRS-aided cellular sensing systems.

On the other hand, security is another critical challenge for wireless sensing due to the inherent broadcast nature of wireless signals. Since IRS has the capability of enhancing wireless signals at desired receivers as well as suppressing them at undesired receivers, it has been applied to improve the communication security in IRS-aided ISAC systems [?], [?]. However, prior works only focused on IRS reflection design to achieve enhanced information/communication security in ISAC systems, but overlooked the important sensing security threat. In practice, the physical characteristics of sensing target (e.g., location and velocity) may be intercepted by unauthorized radar stations (URSs), which thus brings a new sensing security issue. There are two traditional methods for tackling this issue. One method is by designing the target's shape [?], such that it can reflect incident signal to undetectable directions, while this method has limited practical applications due to the specific target shape required. The other method is to wrap the target with electromagnetic (EM) wave absorbing (i.e., EM stealthy) materials [?], which can significantly reduce the reflected radar signal power in all directions. Although the above methods can achieve sensing security against URS, they inevitably render the target invisible to any legitimate radar station (LRS) as well. In addition, other methods have been recently proposed to enable the LRS to detect stealthy target such as increasing the power-aperture product of the LRS, or the number of LRS radar pulses in coherent processing [?]. However, these methods can also be applied by the URS to enhance its target detection. Note that the active IRS sensing approach [?], [?] aforementioned cannot solve the secure sensing problem too, because it has no control over the reflected signal by the target.

In order to improve the target sensing performance while ensuring sensing security at the same time, we propose in this paper a new approach by mounting IRS on the outer surface of the target, namely target-mounted IRS. Specifically, we consider a secure wireless sensing system as shown in Fig. ??, where an LRS aims to detect an aerial target with its echo-surface covered by an IRS, and a URS also intends to detect the same target. The target-mounted IRS can help achieve secure sensing of the target for the LRS as well as against the URS. Specifically, instead of using IRS as additional anchor node in existing IRS-assisted sensing/ISAC systems, mounting IRS on the target can directly control the reflected echo signal from the target. By tuning IRS reflection, the echo signal towards the LRS/URS receiver can be greatly enhanced/suppressed, thus achieving our secure wireless sensing goals. Note that the above IRS reflection design
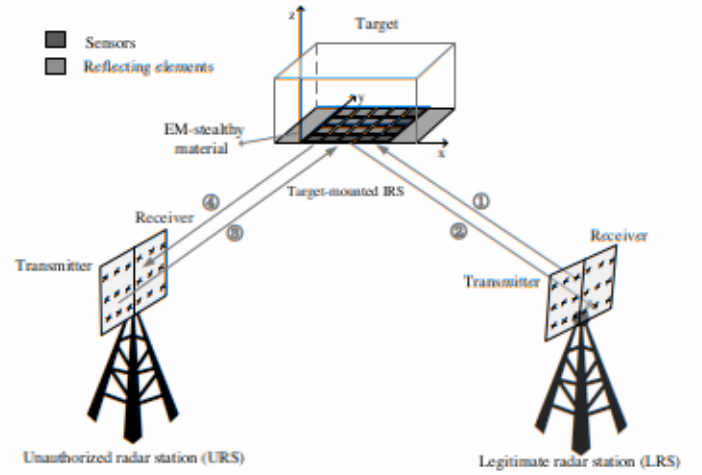

Fig. 1. System model of secure wireless sensing with target-mounted IRS.

generally replies on the knowledge of the angles of arrival (AoAs) of the radar signals from the LRS and/or URS. To achieve this end, we consider installing dedicated sensors along with the reflecting elements at the IRS to enable its acquisition of such information (see Fig. ??). The main contributions of this paper are summarized as follows.

- First, we propose a practical operation protocol for target-mounted IRS to achieve secure wireless sensing. The protocol consists of two steps. In the first step, IRS sensors estimate the LRS/URS channel and waveform parameters with all IRS reflecting elements switched off. Then, in the second step, based on the estimated parameters, IRS reflection is designed to simultaneously boost the received signal at the LRS receiver and suppress that at the URS receiver, thus achieving secure detection of the target.

- Next, to design the IRS reflection for/against the LRS/URS, we formulate new optimization problems for both the cases of short-term and long-term IRS operations with different dynamic reflection capabilities, aiming to maximize the received signal power at the LRS while in the meanwhile keeping that at the URS below a given threshold. However, the formulated optimization problems are non-convex and thus difficult to be solved optimally. To overcome this difficulty, we propose an efficient penalty dual decomposition (PDD)-based algorithm to solve these problems, which yields high-quality suboptimal solutions.

- Finally, we evaluate the performance of our proposed designs via numerical results. The results demonstrate that target-mounted IRS can greatly improve the target's detection accuracy by the LRS in the LRS-only scenario, or degrade the detection performance by the URS in the URS-only scenario, as well as simultaneously enhance/degrade the target sensing at LRS/URS when they are both present. In addition, it is shown that the proposed algorithm achieves comparable performance to the semi-definite relax-

w.r.t. the IRS, respectively. Note that due to the far-field propagation between the LRS/URS and IRS (or target), the above angles apply to all antenna/reflecting/sensor elements on their corresponding UPAs.

Let $\mathbf{d}(B,\zeta)$ denote the one-dimensional (1D) steering vector function of a given 1D array, which is defined as

$$\mathbf{d}(B,\zeta) = \left[1, e^{j\frac{2\pi d}{\lambda}\zeta}, \cdots, e^{j\frac{2\pi d}{\lambda}(B-1)\zeta}\right]^T, \qquad (1)$$

where B denotes the array size, ζ denotes the steering angle, λ denotes the signal wavelength, and d denotes the distance between any two adjacent antenna/reflecting/sensor elements. Accordingly, assuming that the IRS's UPA is parallel to the y-z plane, the two-dimensional (2D) steering vectors at the IRS w.r.t. LRS for the incident and reflected signals can be expressed as

$$\mathbf{a}_l(\phi_L, \eta_L) = \mathbf{d}(N_x, \zeta_l^a) \otimes \mathbf{d}(N_y, \zeta_l^e), \qquad (2)$$

$$\mathbf{a}_l(\pi - \phi_L, \pi + \eta_L) = \mathbf{d}(N_x, \zeta_l^{\bar{a}}) \otimes \mathbf{d}(N_y, \zeta_l^{\bar{e}}), \qquad (3)$$

respectively, where $\zeta_l^a \triangleq \sin(\phi_L)\cos(\eta_L)$, $\zeta_l^e \triangleq \sin(\phi_L)\sin(\eta_L)$, $\zeta_l^{\bar{a}} \triangleq \sin(\pi - \phi_L)\cos(\pi + \eta_L) \triangleq -\sin(\phi_L)\cos(\eta_L)$, and $\zeta_l^{\bar{e}} \triangleq \sin(\pi - \phi_L)\sin(\pi + \eta_L) \triangleq -\sin(\phi_L)\sin(\eta_L)$. Similarly, the 2D steering vectors for the incident and reflected signals at the IRS w.r.t. URS are respectively given by

$$\mathbf{a}_u(\phi_U, \eta_U) = \mathbf{d}(N_x, \zeta_u^a) \otimes \mathbf{d}(N_y, \zeta_u^e), \qquad (4)$$

$$\mathbf{a}_u(\pi - \phi_U, \pi + \eta_U) = \mathbf{d}(N_x, \zeta_u^{\bar{a}}) \otimes \mathbf{d}(N_y, \zeta_u^{\bar{e}}), \qquad (5)$$

where $\zeta_u^a \triangleq \sin(\phi_U)\cos(\eta_U)$, $\zeta_u^e \triangleq \sin(\phi_U)\sin(\eta_U)$, $\zeta_u^{\bar{a}} \triangleq \sin(\pi - \phi_U)\cos(\pi + \eta_U) \triangleq -\sin(\phi_U)\cos(\eta_U)$, and $\zeta_u^{\bar{e}} \triangleq \sin(\pi - \phi_U)\sin(\pi - \eta_U) \triangleq -\sin(\phi_U)\sin(\eta_U)$.

In addition, for the LRS's UPA assumed to be parallel to the y-z plane, its transmit and receive 2D steering vectors w.r.t. the IRS are respectively given by

$$\mathbf{b}(\phi_L, \eta_L) = \mathbf{d}(M_y, \varphi_t^a) \otimes \mathbf{d}(M_z, \varphi_t^e), \qquad (6)$$

$$\mathbf{b}(\pi - \phi_L, \pi + \eta_L) = \mathbf{d}(M_y, \varphi_r^a) \otimes \mathbf{d}(M_z, \varphi_r^e), \qquad (7)$$

where $\varphi_t^a \triangleq \sin(\phi_L)\sin(\eta_L)$, $\varphi_t^e \triangleq \cos(\phi_L)$, $\varphi_r^a \triangleq \sin(\pi - \phi_L)\sin(\pi + \eta_L) \triangleq -\sin(\phi_L)\sin(\eta_L)$, and $\varphi_r^e \triangleq \cos(\pi - \phi_L) \triangleq -\cos(\phi_L)$. Similarly, assuming that the URS is parallel to the y-z plane, its 2D transmit and receive steering vectors are respectively expressed as

$$\mathbf{c}(\phi_U, \eta_U) = \mathbf{d}(D_y, \upsilon_t^a) \otimes \mathbf{d}(D_z, \upsilon_t^e), \qquad (8)$$

$$\mathbf{c}(\pi - \phi_U, \pi + \eta_U) = \mathbf{d}(D_y, \upsilon_r^a) \otimes \mathbf{d}(D_z, \upsilon_r^e), \qquad (9)$$

where $\upsilon_t^a \triangleq \sin(\phi_U)\sin(\eta_U)$, $\upsilon_t^e \triangleq \cos(\phi_U)$, $\upsilon_r^a \triangleq \sin(\pi - \phi_U)\sin(\pi + \eta_U) \triangleq -\sin(\phi_U)\sin(\eta_U)$, and $\upsilon_r^e \triangleq \cos(\pi - \phi_U) \triangleq -\cos(\phi_U)$.

As a result, the IRS→LRS channel $\mathbf{H}_{LI} \in \mathbb{C}^{M \times N}$, LRS→IRS channel $\mathbf{H}_{IL} \in \mathbb{C}^{N \times M}$, IRS→URS channel $\mathbf{H}_{UI} \in \mathbb{C}^{D \times N}$, and URS→IRS channel $\mathbf{H}_{IU} \in \mathbb{C}^{N \times D}$ can be written as

$$\mathbf{H}_{LI} = \alpha_l \mathbf{b}(\pi - \phi_L, \pi + \eta_L)\mathbf{a}_l^H(\pi - \phi_L, \pi + \eta_L), \quad (10)$$

$$\mathbf{H}_{IL} = \alpha_l \mathbf{a}_l(\phi_L, \eta_L)\mathbf{b}^H(\phi_L, \eta_L), \qquad (11)$$

$$\mathbf{H}_{UI} = \alpha_u \mathbf{c}(\pi - \phi_U, \pi + \eta_U)\mathbf{a}_u^H(\pi - \phi_U, \pi + \eta_U), \quad (12)$$

$$\mathbf{H}_{IU} = \alpha_u \mathbf{a}_u(\phi_U, \eta_U)\mathbf{c}^H(\phi_U, \eta_U), \qquad (13)$$

respectively, where $\alpha_l = e^{j\nu_l}\bar{\alpha}_l$ and $\alpha_u = e^{j\nu_u}\bar{\alpha}_u$ with $\bar{\alpha}_l$ and $\bar{\alpha}_u$ denoting the real-valued path gain of the LRS-IRS and URS-IRS LoS channels, respectively, and $\nu_l = \frac{2\pi d_{LI}}{\lambda}$ and $\nu_u = \frac{2\pi d_{UI}}{\lambda}$ being the reference phase of the LRS-IRS and URS-IRS channels, respectively. In the above, d_{LI} and d_{UI} represent the distance between the LRS and target and that between the URS and target, respectively, w.r.t. their reference elements. To characterize the effect of small variations of the LRS-/URS- target distance (i.e., d_{LI} or d_{UI}) due to target position local perturbation on the signal phases ν_l and ν_u, we model ν_l and ν_u as independent and uniformly distributed random variables in $[0, 2\pi)$ [?].

B. Signal Model

As shown in Fig. ??, we assume that the LRS transmits one coherent burst of K_L non-consecutive radar pulses with a constant pulse repetition interval (PRI), denoted as T_L. The duration over which all these signals are reflected by the target and received by the LRS is called the coherent-processing interval (CPI), denoted by T_{CPI}, which is equal to $K_L \times T_L$. The pulse durations of LRS and URS are denoted as t_L and t_U, respectively, with $t_L < T_L$ and $t_U < T_U$, where the PRI of the URS is denoted as T_U. For simplicity, we assume that $T_L = T_U = T$ in this paper[2]. Furthermore, we assume that the target location as well as the PRIs and pulse durations of both LRS and URS remain unchanged during each LRS CPI, but they may change from one CPI to another. In addition, we express the radar pulse waveforms of LRS and URS during each PRI respectively as

$$x(t) = \begin{cases} \sqrt{P_L}p(t), & 0 \leq t \leq t_L \\ 0, & t_L < t \leq T \end{cases} \qquad (14)$$

and

$$s(t) = \begin{cases} \sqrt{P_U}q(t), & 0 \leq t \leq t_U \\ 0, & t_U < t \leq T \end{cases} \qquad (15)$$

where P_L and P_U represent the transmit signal power of LRS and URS, respectively; $p(t)$ and $q(t)$ are the corresponding radar pulses with normalized power, i.e., $\frac{1}{t_L}\int_0^{t_L}|p(t)|^2 dt = 1$ and $\frac{1}{t_U}\int_0^{t_U}|q(t)|^2 dt = 1$.

As shown in Fig. ??, the signal received at the IRS during each LRS CPI may fall into the following three cases depending on whether the received signals from LRS and URS are overlapped or not, i.e., Case 1 (LRS-signal only case): the received signal is from LRS only; Case 2 (URS-signal only case): the received signal is from URS only; and Case 3 (overlapped LRS and URS signal): the received signal consists of overlapped signals from both LRS and URS. For convenience, we use t_o to denote the overlapped signal duration in Case 3, with $0 \leq t_o \leq \min\{t_L, t_U\}$. Note that if $t_o = 0$, then the signals from LRS and URS are completely non-overlapped at the

---

[2]The proposed design in this paper can be extended to the general case of $T_L \neq T_U$, which is omitted due to space limitations.
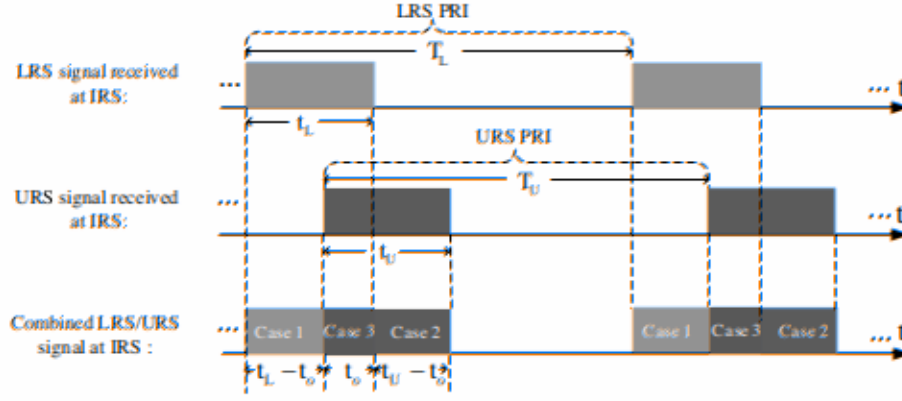
Fig. 3.　Illustration of received LRS/URS signals at IRS.

IRS. Without loss of generality, assuming that the first LRS signal arrives at IRS before that of URS during each LRS CPI, we present the signal models for the above three cases in the following, respectively.

First, for Case 1 (i.e., $0 \leq t \leq t_L - t_o$) with only the LRS signal reflected by the IRS, the signals received by the LRS receiver through the link ①→② in Fig. ?? (i.e., LRS→target/IRS→LRS) and the URS receiver via the link ①→④ in Fig. ?? (i.e., LRS→target/IRS→URS) at time t can be respectively expressed as

$$y_{LL}(t) = \mathbf{w}_L^T \mathbf{H}_{LI} \mathrm{diag}(\boldsymbol{\theta}) \mathbf{H}_{IL} \mathbf{w}_L x(t) + z_L(t), \qquad (16)$$

$$y_{LU}(t) = \mathbf{w}_U^T \mathbf{H}_{UI} \mathrm{diag}(\boldsymbol{\theta}) \mathbf{H}_{IL} \mathbf{w}_L x(t) + z_U(t), \qquad (17)$$

where $z_L(t)$ and $z_U(t)$ denote the additive white Gaussian noise (AWGN) with zero mean and average power σ_L^2 and σ_U^2, respectively, $\mathbf{w}_L \in \mathbb{C}^{M \times 1}$ and $\mathbf{w}_U \in \mathbb{C}^{D \times 1}$ are the transmit beamformers at LRS and URS, respectively, and $\mathbf{w}_L^T \in \mathbb{C}^{1 \times M}$ and $\mathbf{w}_U^T \in \mathbb{C}^{1 \times D}$ denote their matching receive beamformers at LRS and URS, respectively.

Second, for Case 2 (i.e., $t_L < t \leq t_L + t_U - t_o$) with only the URS signal reflected by the IRS, the signals received by the LRS receiver via the link ③→② in Fig. ?? (i.e., URS→target/IRS→LRS) and the URS receiver through the link ③→④ in Fig. ?? (i.e., URS→target/IRS→URS) are respectively given by

$$y_{UL}(t) = \mathbf{w}_L^T \mathbf{H}_{LI} \mathrm{diag}(\boldsymbol{\theta}) \mathbf{H}_{IU} \mathbf{w}_U s(t) + z_L(t), \qquad (18)$$

$$y_{UU}(t) = \mathbf{w}_U^T \mathbf{H}_{UI} \mathrm{diag}(\boldsymbol{\theta}) \mathbf{H}_{IU} \mathbf{w}_U s(t) + z_U(t). \qquad (19)$$

Third, for Case 3 (i.e., $t_L - t_o < t \leq t_L$) with the overlapped signal reflected by the IRS, the signals received by the LRS receiver through both links ①→② and ③→② in Fig. ?? and the URS receiver via both links ①→④ and ③→④ in Fig. ?? are respectively expressed as

$$y_{OL}(t) = \mathbf{w}_L^T \mathbf{H}_{LI} \mathrm{diag}(\boldsymbol{\theta}) \mathbf{H}_{IL} \mathbf{w}_L x(t)$$
$$+ \mathbf{w}_L^T \mathbf{H}_{LI} \mathrm{diag}(\boldsymbol{\theta}) \mathbf{H}_{IU} \mathbf{w}_U s(t) + z_L(t), \qquad (20)$$

$$y_{OU}(t) = \mathbf{w}_U^T \mathbf{H}_{UI} \mathrm{diag}(\boldsymbol{\theta}) \mathbf{H}_{IU} \mathbf{w}_U s(t)$$
$$+ \mathbf{w}_U^T \mathbf{H}_{UI} \mathrm{diag}(\boldsymbol{\theta}) \mathbf{H}_{IL} \mathbf{w}_L x(t) + z_U(t). \qquad (21)$$

In practice, the performance of target detection/estimation (e.g., detecting the presence of a target or estimating a target's AoA) improves with the increase of

received signal power [?]. This is intuitively expected, since larger signal power results in higher signal-to-noise ratio (SNR) of the received echo signal, thus leading to lower detection/estimation error. Therefore, we use the received signal powers at the LRS/URS as the performance metric for their target detection/estimation, and derive them for the above three cases, respectively, as follows.

First, according to (??) and (??), the received signal powers at LRS and URS in Case 1 are respectively given by

$$Q_{LL} = |\mathbf{w}_L^T \mathbf{H}_{LI} \mathrm{diag}(\boldsymbol{\theta}) \mathbf{H}_{IL} \mathbf{w}_L x(t)|^2$$
$$= |\bar{\alpha}_l \mathbf{w}_L^T \mathbf{b}(\pi - \phi_L, \pi + \eta_L) \mathbf{u}^H \boldsymbol{\theta} \bar{\alpha}_l \mathbf{b}^H(\phi_L, \eta_L) \mathbf{w}_L x(t)|^2$$
$$= \frac{Q_{LS}^2}{P_L} \times |\mathbf{u}^H \boldsymbol{\theta}|^2, \qquad (22)$$

and

$$Q_{LU} = |\mathbf{w}_U^T \mathbf{H}_{UI} \mathrm{diag}(\boldsymbol{\theta}) \mathbf{H}_{IL} \mathbf{w}_L x(t)|^2$$
$$= |\bar{\alpha}_u \mathbf{w}_U^T \mathbf{c}(\pi - \phi_U, \pi + \eta_U) \mathbf{v}^H \boldsymbol{\theta} \bar{\alpha}_l \mathbf{b}^H(\phi_L, \eta_L) \mathbf{w}_L x(t)|^2$$
$$= \frac{Q_{LS} Q_{US}}{P_U} \times |\mathbf{v}^H \boldsymbol{\theta}|^2, \qquad (23)$$

with

$$\mathbf{u} = \mathbf{a}_l(\pi - \phi_L, \pi + \eta_L) \odot \mathbf{a}_l^*(\phi_L, \eta_L)$$
$$\triangleq \mathbf{d}(N_x, \zeta_l^{\bar{a}} - \zeta_l^a) \otimes \mathbf{d}(N_y, \zeta_l^{\bar{e}} - \zeta_l^e) \in \mathbb{C}^{N \times 1}, \quad (24)$$
$$\mathbf{v} = \mathbf{a}_u(\pi - \phi_U, \pi + \eta_U) \odot \mathbf{a}_l(\phi_L, \eta_L)$$
$$\triangleq \mathbf{d}(N_x, \zeta_u^{\bar{a}} - \zeta_l^a) \otimes \mathbf{d}(N_y, \zeta_u^{\bar{e}} - \zeta_l^e) \in \mathbb{C}^{N \times 1}, \quad (25)$$
$$Q_{LS} = |\bar{\alpha}_l \mathbf{b}^H(\phi_L, \eta_L) \mathbf{w}_L x(t)|^2, \qquad (26)$$
$$Q_{US} = |\bar{\alpha}_u \mathbf{w}_U^T \mathbf{c}(\pi - \phi_U, \pi + \eta_U) s(t)|^2, \qquad (27)$$

where $|\mathbf{u}^H \boldsymbol{\theta}|^2$ and $|\mathbf{v}^H \boldsymbol{\theta}|^2$ depend on the IRS reflection, i.e., $\boldsymbol{\theta}$, and Q_{LS} and Q_{US} represent the received signal powers at IRS from LRS and URS, respectively.

Similarly, based on (??) and (??), the received signal powers at LRS and URS in Case 2 are respectively

$$Q_{UL} = |\mathbf{w}_L^T \mathbf{H}_{LI} \mathrm{diag}(\boldsymbol{\theta}) \mathbf{H}_{IU} \mathbf{w}_U s(t)|^2$$
$$= |\bar{\alpha}_l \mathbf{w}_L^T \mathbf{b}(\pi - \phi_L, \pi + \eta_L) \mathbf{r}^H \boldsymbol{\theta} \bar{\alpha}_u \mathbf{c}^H(\phi_U, \eta_U) \mathbf{w}_U s(t)|^2$$
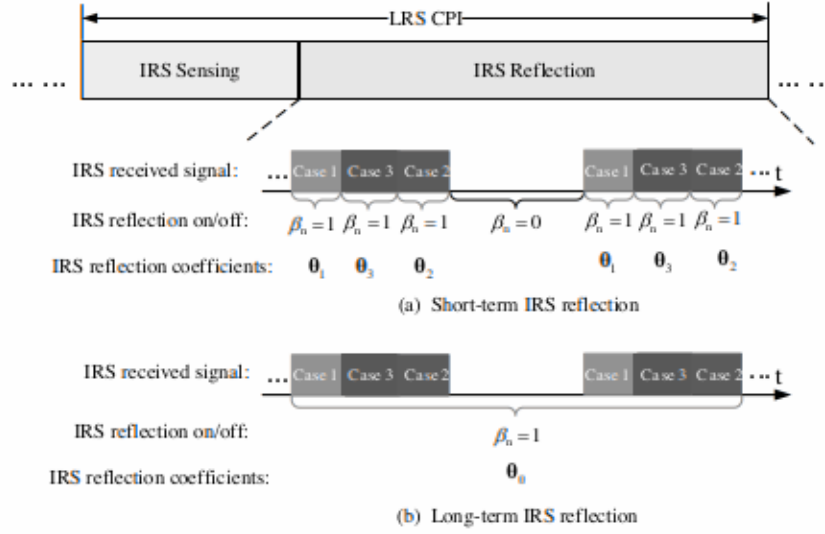$$= \frac{Q_{LS} Q_{US}}{P_L} \times |\mathbf{r}^H \boldsymbol{\theta}|^2, \qquad (28)$$

Fig. 4. Proposed protocol for secure wireless sensing with the target-mounted IRS.

A. Short-Term IRS Reflection Design

For short-term IRS reflection, we need to optimize the IRS reflection separately for three cases within each LRS CPI, namely, LRS-signal only, URS-signal only, and overlapped LRS and URS signal. Specifically, for the LRS-signal-only case, we aim to maximize the power of the IRS-reflected LRS signal over the LRS→IRS→LRS link, while keeping that over the LRS→IRS→URS link below a certain level, by optimizing the IRS reflection phase shifts. Consequently, based on (??) and (??), the optimization problem can be formulated as

$$(\mathcal{P}_1): \max_{\boldsymbol{\theta}_1} \quad \underbrace{Q_{LS}^2 \times |\mathbf{u}^H \boldsymbol{\theta}_1|^2}_{\text{LRS→IRS→LRS}} \tag{38a}$$

$$\text{s.t.} \quad \underbrace{\frac{Q_{LS}Q_{US}}{P_{U,\min}} \times |\mathbf{v}^H \boldsymbol{\theta}_1|^2}_{\text{LRS→IRS→URS}} \leq \gamma, \tag{38b}$$

$$|\theta_{1,n}| = 1, n = 1, \cdots, N, \tag{38c}$$

where $P_{U,\min}$ denotes the minimum value of P_U which is assumed to be known and denotes the maximum received signal power threshold at the LRS, below which the LRS cannot achieve its desired target detection/estimation performance.

Next, for the URS-signal-only case, our goal is to maximize the power of IRS-reflected URS signal over the URS→IRS→LRS link for exploiting the URS's radar signal for the LRS's target detection, subject to that over the URS→IRS→URS link being below the given threshold γ. According to (??) and (??), the IRS reflection phase shifts can be optimized by solving the following problem,

$$(\mathcal{P}_2): \max_{\boldsymbol{\theta}_2} \quad \underbrace{Q_{LS}Q_{US} \times |\mathbf{r}^H \boldsymbol{\theta}_2|^2}_{\text{URS→IRS→LRS}} \tag{39a}$$

$$\text{s.t.} \quad \underbrace{\frac{Q_{US}^2}{P_{U,\min}} \times |\mathbf{g}^H \boldsymbol{\theta}_2|^2}_{\text{URS→IRS→URS}} \leq \gamma, \tag{39b}$$

$$|\theta_{2,n}| = 1, n = 1, \cdots, N. \tag{39c}$$

Last, for the case of overlapped LRS and URS signal, we aim to maximize the average power of IRS-reflected overlapped LRS and URS signal at the LRS receiver, while keeping that at the URS receiver below γ. To achieve this, we can formulate the following IRS reflection phase shifts optimization problem based on (??) and (??),

$$(\mathcal{P}_3): \max_{\boldsymbol{\theta}_3} \quad \underbrace{Q_{LS}^2 \times |\mathbf{u}^H \boldsymbol{\theta}_3|^2}_{\text{LRS→IRS→LRS}} + \underbrace{Q_{LS}Q_{US} \times |\mathbf{r}^H \boldsymbol{\theta}_3|^2}_{\text{URS→IRS→LRS}} \tag{40a}$$

$$\text{s.t.} \quad \underbrace{\frac{Q_{US}^2}{P_{U,\min}} \times |\mathbf{g}^H \boldsymbol{\theta}_3|^2}_{\text{URS→IRS→URS}} + \underbrace{\frac{Q_{LS}Q_{US}}{P_{U,\min}} \times |\mathbf{v}^H \boldsymbol{\theta}_3|^2}_{\text{LRS→IRS→URS}} \leq \gamma, \tag{40b}$$

$$|\theta_{3,n}| = 1, n = 1, \cdots, N. \tag{40c}$$

Remark 1: The estimates of LRS/URS AoAs $\{\phi_L, \eta_L\}$ and $\{\phi_U, \eta_U\}$ in Step I of the proposed protocol are required for constructing the vectors $\mathbf{u}$, $\mathbf{v}$, $\mathbf{r}$, and $\mathbf{g}$ involved in problems $(\mathcal{P}_1)$ to $(\mathcal{P}_3)$. In addition, the estimates of received signal powers from LRS and URS at IRS, i.e., Q_{LS} and Q_{US} in Step I are also needed for formulating the objective functions and constraints in $(\mathcal{P}_1)$ to $(\mathcal{P}_3)$.

B. Long-Term IRS Reflection Design

The objective of long-term IRS reflection is to maximize the total energy of IRS-reflected LRS signal with duration t_L and URS signal with duration t_U at the LRS receiver, while keeping their overlapped signal peak power (in Case 3 by assuming the worst case of $t_o > 0$) at the URS receiver below the given threshold γ. Similar to $(\mathcal{P}_3)$, the IRS reflection phase shifts during Step II can be optimized by the following problem,

$$(\mathcal{P}_4): \max_{\boldsymbol{\theta}_0} \quad \underbrace{t_L Q_{LS}^2 \times |\mathbf{u}^H \boldsymbol{\theta}_0|^2}_{\text{LRS→IRS→LRS}} + \underbrace{t_U Q_{LS}Q_{US} \times |\mathbf{r}^H \boldsymbol{\theta}_0|^2}_{\text{URS→IRS→LRS}} \tag{41a}$$

general. To circumvent this difficulty, we approximate the convex function $|\mathbf{q}_i^H \boldsymbol{\theta}|^2$ by its first-order Taylor expansion at a given point $\tilde{\boldsymbol{\theta}}$, denoted by $\underline{q}_i(\boldsymbol{\theta}, \tilde{\boldsymbol{\theta}})$, i.e.,

$$|\mathbf{q}_i^H \boldsymbol{\theta}|^2 \geq \underline{q}_i(\boldsymbol{\theta}, \tilde{\boldsymbol{\theta}}) \triangleq 2\Re(\varepsilon_i^H \boldsymbol{\theta}) + \bar{\xi}_i, \qquad (47)$$

where $\varepsilon_i \triangleq \mathbf{q}_i^H \tilde{\boldsymbol{\theta}} \mathbf{q}_i^H$ and $\bar{\xi}_i = -|\mathbf{q}_i^H \tilde{\boldsymbol{\theta}}|^2$. Therefore, we obtain the following problem,

$$(\mathcal{P}_9) : \min_{\boldsymbol{\theta}} \ -2\sum_{i=1}^2 \Re(\varepsilon_i^H \boldsymbol{\theta}) - \sum_{i=1}^2 \bar{\xi}_i + \frac{1}{2\rho}\|\boldsymbol{\theta} - \boldsymbol{\vartheta} + \rho\boldsymbol{\lambda}\|_2^2 \tag{48a}$$

$$\text{s.t.} \ \sum_{i=1}^2 |\mathbf{h}_i^H \boldsymbol{\theta}|^2 \leq \gamma, \tag{48b}$$

$$|\theta_n| \leq 1, n = 1, \cdots, N. \tag{48c}$$

Problem $(\mathcal{P}_9)$ is a convex optimization problem, which can be solved efficiently via existing software, e.g., CVX [?]. By repeatedly solving $(\mathcal{P}_9)$, and setting the point for Taylor expansion, i.e., $\tilde{\boldsymbol{\theta}}$, in each iteration as the optimal solution obtained in the previous iteration, the above procedure generates a sequence of solutions that converge to a Karush-Kuhn-Tucker (KKT) solution of $(\mathcal{P}_8)$ [?].

On the other hand, when $\boldsymbol{\theta}$ is given, $\boldsymbol{\vartheta}$ can be updated by solving the following problem,

$$(\mathcal{P}_{10}) : \min_{\boldsymbol{\vartheta}} \ \|\boldsymbol{\theta} - \boldsymbol{\vartheta} + \rho\boldsymbol{\lambda}\|_2^2 \tag{49a}$$

$$\text{s.t.} \ |\vartheta_n| = 1, n = 1, \cdots, N, \tag{49b}$$

for which the optimum is attained when the elements of $\boldsymbol{\vartheta}$ satisfy the following condition,

$$\vartheta_n^* = \angle(\theta_n + \rho\lambda_n). \tag{50}$$

In summary, the inner loop alternatively updates $\boldsymbol{\vartheta}$ and $\boldsymbol{\theta}$ until convergence is reached.

Next, we consider the outer loop, where the dual variable $\boldsymbol{\lambda}$ can be updated by

$$\boldsymbol{\lambda} := \boldsymbol{\lambda} + \frac{1}{\rho}(\boldsymbol{\theta} - \boldsymbol{\vartheta}). \tag{51}$$

The above PDD-based algorithm for solving $(\mathcal{P}_5)$ is summarized in Algorithm 1. In step 17 of Algorithm 1, $c < 1$ is a positive constant scaling factor that is used to enlarge the value of the penalty term involved in problem $(\mathcal{P}_7)$ in each outer iteration.

Finally, we compare the complexity of the proposed PDD-based method and SDR-based method in [?]. By carefully checking the iterative process in Algorithm 1, its computational complexity is found to be dominated by that for solving problem $(\mathcal{P}_9)$, which has a complexity of order $\mathcal{O}(N^2)$. Therefore, the overall complexity of Algorithm 1 can be shown in the order of $\mathcal{O}(J_0 J_1 J_2 N^2)$, where J_0 and J_1 denote the maximum outer and inner iteration numbers, and J_2 is the number of iterations for solving $(\mathcal{P}_9)$. In contrast, the computational complexity of the SDR-based method can be shown in the order of $\mathcal{O}(N^{6.5})$ [?]. Thus, the complexity of the proposed Algorithm 1 is much lower than the SDR-based method,

---

Algorithm 1: PDD-based Algorithm for Solving $(\mathcal{P}_5)$

1   Initialize $\boldsymbol{\vartheta}^0$, $\boldsymbol{\theta}^0$, $\boldsymbol{\lambda}^0$, $\tilde{\boldsymbol{\theta}}$, $k = 1$, $c < 1$, and $\epsilon_{\text{out}} > 0$;
2   **repeat**
3     $t = 0$;
4   Set $\boldsymbol{\vartheta}^{k-1,0} = \boldsymbol{\vartheta}^{k-1}$, $\boldsymbol{\theta}^{k-1,0} = \boldsymbol{\theta}^{k-1}$, $\boldsymbol{\lambda}^{k-1,0} = \boldsymbol{\lambda}^{k-1}$;
5   **repeat**
6       $l = 0$;
7   **repeat**
8   Update $\boldsymbol{\theta}^{k-1,t+1}$ by solving problem $(\mathcal{P}_9)$;
9         $l \leftarrow l + 1$;
10        $\tilde{\boldsymbol{\theta}} = \boldsymbol{\theta}^{k-1,t+1}$;
11   **until** *convergence*;
12   Update $\boldsymbol{\vartheta}^{k-1,t+1}$ according to (50);
13       $t \leftarrow t + 1$;
14   **until** *convergence*;
15   Set $\boldsymbol{\vartheta}^k = \boldsymbol{\vartheta}^{k-1,t}$, $\boldsymbol{\theta}^k = \boldsymbol{\theta}^{k-1,t}$;
16     $\boldsymbol{\lambda}^{k+1} = \boldsymbol{\lambda}^k + \frac{1}{\rho^k}(\boldsymbol{\theta}^k - \boldsymbol{\vartheta}^k)$;
17     $\rho^{k+1} = c\rho^k$;
18     $k \leftarrow k + 1$;
19 **until** $\|\boldsymbol{\vartheta}^k - \boldsymbol{\theta}^k\|_2$ *is below a certain threshold* ϵ_{out};

---

especially for large-size IRS with large values of N.

V. Numerical Results

In this section, we evaluate the performance of our proposed target-mounted IRS enabled secure wireless sensing design via numerical results. In the following simulations, the radar pulse waveforms of LRS and URS are given by $x(t) = \exp(j\pi B t^2/t_L)$ and $s(t) = \exp(j\pi B t^2/t_U)$, respectively, with the signal bandwidth $B = 100$ MHz. For simplicity, we consider uniform linear array (ULA) for the IRS, LRS, and URS, where the numbers of antennas at the ULRS and URS are $M = 64$ and $D = 64$, respectively; the number of IRS reflecting elements and sensors are $N = 64$ and $L = 15$, respectively; the wavelength is $\lambda = 0.2$ m; the target is located at 0 horizontally and from the IRS, and the transmit powers of LRS and URS are set as $P_L = P_U = 30$ dBm. The target and the IRS-target distances are set as $d_L = 20$ m and $d_U = 20$ m, respectively; the LRS/URS PRI is $T = 100$ μs with the pulse durations of $t_E = 30$ μs and $t_U = 30$ μs; the total physical size of IRS is set $N d^2$; the target echo surface is set as A_i, $i = 1, 2$. Size of the target echo surface is larger than that of the IRS; the RCS of the target is set $\kappa = \frac{4\pi A^2}{\lambda^2}$; and the IRS element separation is $d = \lambda/10$ unless otherwise stated. For the purpose of exposition, we first assume that the IRS/LRS/URS channel and waveform parameters are perfectly estimated by the IRS sensors, while the effect of their imperfect estimation on the performance are then evaluated.

For comparison, we consider the following benchmark schemes:

1) Random Phase Shift: We assume that each IRS reflecting element takes a random phase shift inde-

Fig. 5. Received signal power at LRS versus LRS transmit beam direction.

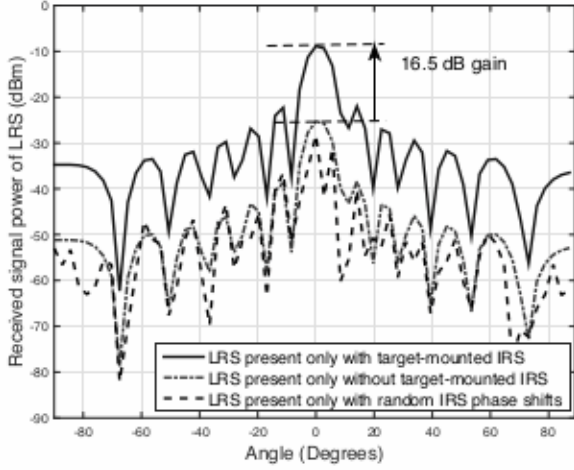Fig. 6. Received signal power at URS versus URS transmit beam direction.

pendently and uniformly distributed in $[0, 2\pi)$, based on which we obtain the received signal power at LRS or URS.

2) No Target-Mounted IRS: There is no IRS mounted on the target, as in the traditional sensing system.

3) SDR-based Method: Problem ($\mathcal{P}_5$) is first transformed into an semidefinite programming (SDP) problem by applying SDR and dropping the nonconvex rank-one constraint, i.e., $\text{rank}(\boldsymbol{\theta\theta}^H) = 1$. The resulting convex SDP is then optimally solved by CVX [?] with 10000 Gaussian randomizations generated to find the best rank-1 feasible solution for ($\mathcal{P}_5$).

A. LRS Present Only

First, we consider the special case where only the LRS is present in the system to detect the target. In this case, there is no security concern and our objective is to maximize the power of reflected echo signal from the target/IRS towards the LRS receiver for enhancing its target sensing performance, by optimizing the IRS reflection. This problem can be formulated by setting $\mathbf{q}_1 = \sqrt{Q_{LS}^2}\mathbf{u}$, $\mathbf{q}_2 = \mathbf{h}_1 = \mathbf{h}_2 = \mathbf{0}$ in problem ($\mathcal{P}_5$). It can be easily shown that the optimal solution to this problem is given by $\boldsymbol{\theta}_L^o = \mathbf{u}$. This implies that the optimal IRS reflection should align the reflected signal from IRS with its AoA to IRS for maximizing the signal power at the LRS receiver to improve its target detection/estimation accuracy.

Fig. ?? compares the received signal power at the LRS receiver under different schemes versus the LRS transmit beam direction (i.e., by setting different $\mathbf{w}_L$). In this simulation, we keep the location of the target fixed, while the LRS transmitter scans different angles in the target space via transmit beamforming based on the discrete Fourier transform (DFT) of size N. First, it is shown that, despite that the IRS has a smaller size than the target's echo surface, the received signal power at LRS with target-mounted IRS yields about 16.5 dB gain over
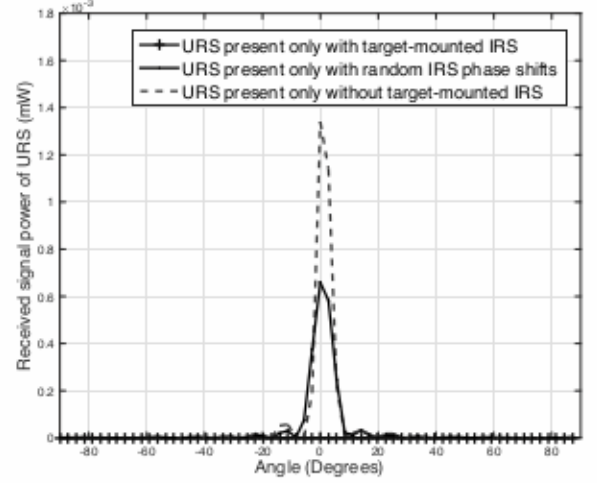
the traditional sensing without IRS at the target angle. This is because when the LRS beam hits the direction of the target, the target-mounted IRS provides a strong passive beamforming gain for the echo signal, which is not available for the target without IRS. Second, with target-mounted IRS, the proposed reflection design achieves significantly improved signal power at the LRS receiver over the scheme with random IRS phase shifts, which is lack of IRS passive beamforming gain. Third, it is observed that the scheme without target-mounted IRS performs better than the scheme with random IRS phase shifts. This is because, although the reflected signals in both schemes are not directional to the LRS, the size of the target echo surface is larger than that of the IRS, thus resulting in more reflected signal power at the LRS receiver on average.

B. URS Present Only

Next, we consider another special case where only the URS is present in the system to detect the same target. In this case, we aim to minimize the power of echo signal from the target/IRS towards the URS receiver by optimizing the IRS reflection. Accordingly, the optimization problem can be formulated as

$$\min_{\boldsymbol{\theta}} \quad \underbrace{|\mathbf{g}^H\boldsymbol{\theta}|^2}_{\text{URS}\to\text{IRS}\to\text{URS}}$$
$$\text{s.t.} \quad |\theta_n| = 1, n = 1, \cdots, N. \qquad (52)$$

By exploiting the structure of LoS-based channel vector $\mathbf{g}$ given in (??), we show in the following proposition a closed-form optimal solution to the above problem.

Proposition 1: The optimal solution to problem (??) is given by

$$\boldsymbol{\theta}_U^o = \boldsymbol{\theta}_x^o \otimes \boldsymbol{\theta}_y^o, \qquad (53)$$

with $\boldsymbol{\theta}_x^o = \mathbf{d}(N_x, \varsigma_x^o)$ and $\boldsymbol{\theta}_y^o = \mathbf{d}(N_y, \varsigma_y^o)$, where $\varsigma_x^o = (\zeta_u^{\bar{a}} - \zeta_u^a) + \frac{\lambda}{N_x d}i_x$, $i_x = 1, 2, \cdots, N_x - 1$ and $\varsigma_y^o = (\zeta_u^{\bar{e}} - \zeta_u^e) + \frac{\lambda}{N_y d}i_y$, $i_y = 1, 2, \cdots, N_y - 1$.
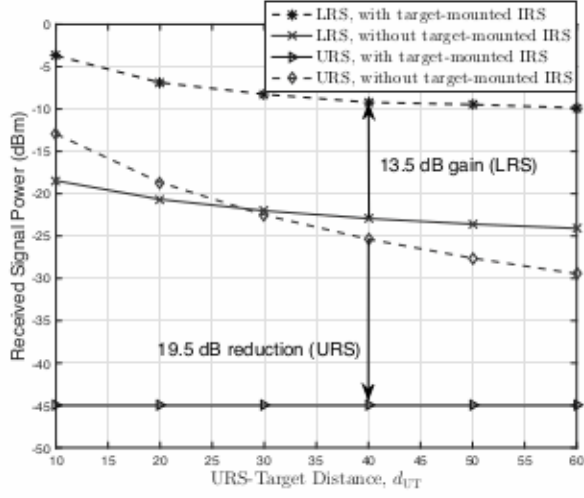
Proof: Please refer to Appendix A. $\blacksquare$

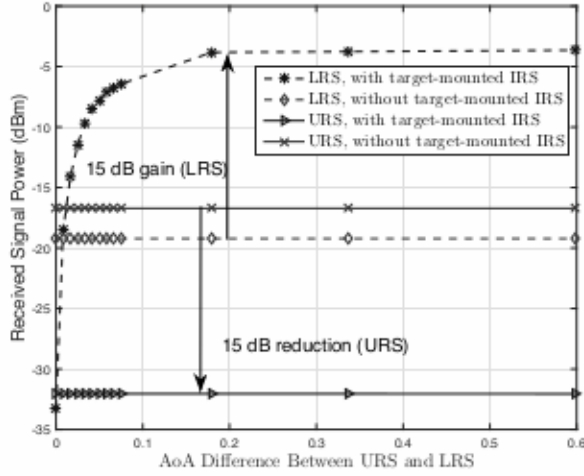Fig. 9. The performance of the proposed scheme versus URS-target distance.

Fig. 11. Received signal power at LRS versus the LRS/URS signal overlapping ratio with short-term or long-term IRS reflection.

Fig. 10. The performance of the proposed scheme versus the AoA difference between URS and LRS.

Fig. 12. Effect of imperfect IRS sensor angle estimation to LRS/URS received signal power with short-term or long-term IRS reflection.

d_{LT}. This demonstrates the advantage of using URS radar signals for the LRS target's detection, especially when the LRS is located far away from the target and its own radar signal is severely attenuated due to the increased LRS-target distance.

In Fig. ??, we keep the AoAs from LRS and URS to target/IRS fixed, and plot the received signal powers at LRS and URS with or without target-mounted IRS versus the distance between the URS and target. For the case with target-mounted IRS, the proposed PDD-based algorithm is applied with short-term IRS reflection. It is observed that compared to the case without target-mounted IRS, the proposed design with target-mounted IRS can significantly enhance the received signal power at LRS and reduce that at URS at the same time, for a large range of URS-target distance values.

In Fig. ??, we keep LRS-target distance and URS-target distance fixed, and plot the received signal powers at LRS and URS with or without target-mounted IRS versus the
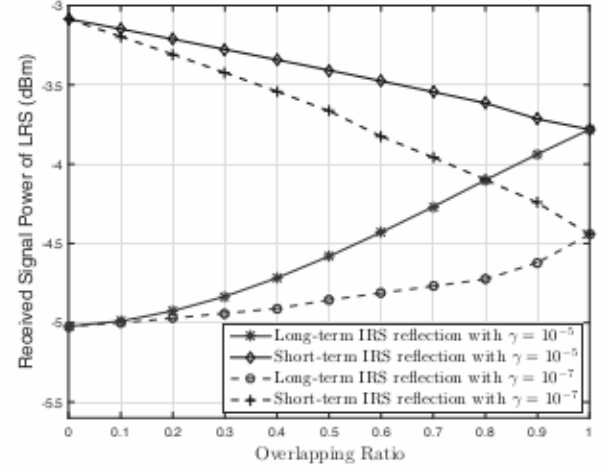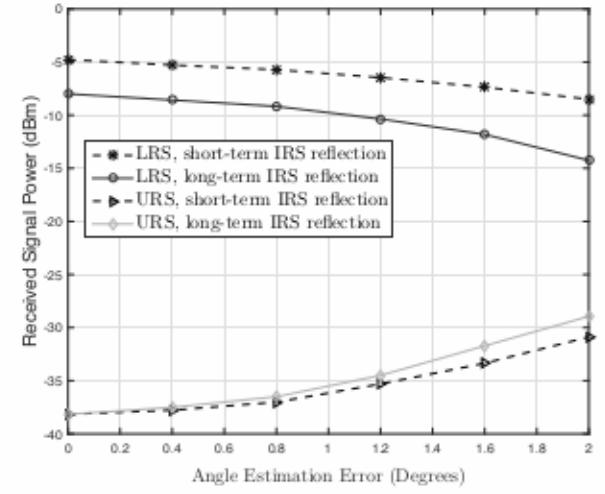
AoA difference between LRS and URS. It is shown that for the scheme without target-mounted IRS, received power at LRS and URS are constant due to fixed LRS-target and URS-target distances, regardless of their AoA to the target/IRS. In contrast to the proposed design with target-mounted IRS can achieve greatly enhanced/suppressed power at LRS/URS receivers, provided that the AoA difference between LRS and URS is sufficiently large, say, larger than 0.1 radian (rad).

Fig. ?? compares the performance of long-term versus short-term IRS reflection for the proposed target-mounted IRS design under different ratios of the LRS/URS overlapping signal duration to that of the LRS/URS pulse duration, i.e., t_o/t_U by assuming $t_L = t_U = 30$ us. It is observed that the received signal power at LRS with long-term IRS reflection is upper-bounded by that with short-term IRS reflection, as expected. In addition, as the LRS/URS signal overlapping ratio increases, the received signal power at LRS with long-term IRS reflection